Modeling of Thermoelectric Properties of Semi-Conductor Thin Films With Quantum and Scattering Effects

A. Bulusu
Interdisciplinary Program in Materials Science,
Vanderbilt University,
Nashville, TN 37235

D. G. Walker[1]
Department of Mechanical Engineering,
Vanderbilt University,
Nashville, TN 37235
e-mail: greg.walker@vanderbilt.edu

Several new reduced-scale structures have been proposed to improve thermoelectric properties of materials. In particular, superlattice thin films and wires should decrease the thermal conductivity, due to increased phonon boundary scattering, while increasing the local electron density of states for improved thermopower. The net effect should be increased ZT, the performance metric for thermoelectric structures. Modeling these structures is challenging because quantum effects often have to be combined with noncontinuum effects and because electronic and thermal systems are tightly coupled. The nonequilibrium Green's function (NEGF) approach, which provides a platform to address both of these difficulties, is used to predict the thermoelectric properties of thin-film structures based on a limited number of fundamental parameters. The model includes quantum effects and electron-phonon scattering. Results indicate a 26–90 % decrease in channel current for the case of near-elastic, phase-breaking, electron-phonon scattering for single phonon energies ranging from 0.2 meV to 60 meV. In addition, the NEGF model is used to assess the effect of temperature on device characteristics of thin-film heterojunctions whose applications include thermoelectric cooling of electronic and optoelectronic systems. Results show the predicted Seebeck coefficient to be similar to measured trends. Although superlattices have been known to show reduced thermal conductivity, results show that the inclusion of scattering effects reduces the electrical conductivity leading to a significant reduction in the power factor ($S^2\sigma$).
[DOI: 10.1115/1.2709962]

Keywords: quantum simulation, thermoelectric, electron-phonon scattering

1 Introduction

Quantum-well superlattices have been proposed as a nanoscale structure that could potentially lead to dramatic increases in the performance of thermoelectric devices [1,2]. The use of quantum-well structures as thermoelectric materials is believed to enhance the thermoelectric figure of merit ($ZT=S^2\sigma T/\kappa$, where S is the Seebeck coefficient, σ is the electrical conductivity, and κ is the thermal conductivity) for several reasons: (i) The reduced dimensionality of a two-dimensional (2D) quantum well increases the local electron density of states per unit volume near the Fermi energy leading to an increase in the Seebeck coefficient [3]. (ii) The introduction of material interfaces promotes phonon scattering, which theoretically reduces the effective thermal conductivity. (iii) Phonon interference effects caused by phonon-interface scattering give rise to phonon band gaps at the interface of the thin films in a superlattice, which further reduces phonon transport [4]. The net result of these effects is a structure with a theoretically higher ZT than its bulk counterparts. Consequently, several researchers have experimentally investigated the role of quantum well, wire, and dot [5–9] superlattice layers on thermal transport. For example, Chen [10,11] has studied the phonon transport in Si/Ge superlattices using the Boltzmann transport equation for phonons. Phonon interface scattering was included through a combination of diffuse and specular scattering. They found that the greatest temperature drop occurred at the interfaces rather than within the layers due to a combination of diffuse and inelastic scattering processes thus developing the concept of phonon engineering to build structures having low thermal conductivity. Based on these findings alone, superlattices should improve the performance of thermoelectric devices compared to bulk materials.

Unfortunately, observations especially in the case of Si/Ge superlattices have not been able to recognize the presumed benefits of superlattice thermoelectric devices despite a theoretically predicted and experimentally observed reduction in the thermal conductivity of a superlattice compared to its bulk counterpart [3,5]. If we assume the thermal conductivity can be reduced by introducing phonon scattering sites, then the lack of performance must be attributed to a corresponding reduction in electrical properties (both σ and S). Normally, the electrical properties are not expected to be affected by the lattice structure because of the disparity between electron and phonon wavelengths and mean free paths [12]. Nevertheless, this presumption does not consider confinement, interface scattering of electrons, and electron-phonon scattering in the lattice. Therefore, to understand the effects of a lattice structure on thermoelectric performance, the Seebeck coefficient and electrical conductivity of a heterojunction are investigated using a nonequilibrium Green's function (NEGF) technique. The approach incorporates quantum as well as scattering effects, both of which are important in describing the physical behavior of confined structures.

The physical features that differentiate nanoscale device modeling from bulk modeling are quantum confinement and noncontinuum effects. Quantum effects usually dominate when the device length scales are of the order of the deBroglie wavelength. Quantum effects can have a detrimental impact in the form of leakage currents in very small transistors [13] or can be very

[1]Corresponding author.

Contributed by the Heat Transfer Division of ASME for publication in the JOURNAL OF HEAT TRANSFER. Manuscript received March 3, 2006; final manuscript received July 29, 2006. Review conducted by Jayathi Murthy.

useful as a high-performance alternative to very large-scale integration (VLSI) [14] in the form of resonant tunneling diodes. Noncontinuum effects can significantly influence charge as well as thermal transport in devices when characteristic lengths are of the order of the mean free path of energy carriers (~10–100 nm) [15]. For example, films as large as 0.5 μm have exhibited a reduction in thermal conductivity by as much as 30% [16] compared to bulk quantities at room temperature. Similarly, wires of decreasing diameter (150–25 nm) show dramatically reduced thermal conductivity as well as strong temperature dependence [17]. In terms of electrons, noncontinuum effects, particularly "hot electron" effects, have been studied for their impact on device performance [18].

The most common approach for thermal modeling at reduced scales is based on the Boltzmann transport equation (BTE). Tractable solutions of the BTE include limited carrier scattering through a relaxation-time approximation, where the system is considered to be only slightly perturbed from equilibrium. Numerical solutions to the BTE are possible using Monte Carlo techniques [19] in which particle distributions are solved using stochastic processes. Mazumder and Majumdar [20] describes such an approach that includes phonon dispersion and various phonon modes independently. For coupled solutions, an electrothermal model based on moments of the BTE for phonons and electrons was developed to simulate electron-phonon interactions [21]. This nonequilibrium approach has shown that the energy distributions for optical and acoustic phonons differ significantly, suggesting that nonequilibrium behavior is very different from continuum behavior. Using a similar model, Raman et al. [22] showed that nonequilibrium significantly affects the location and generation of the hot spot in microelectronic power devices. To remove the gray assumption in moment-based solutions, an unstructured finite-volume discrete ordinates scheme has been used to solve the BTE with spectral information [23]. Isotropic scattering in the form of impurity and Umklapp scattering was considered, and a favorable match with exact solutions was found. However, in spite of all the progress made in small-scale device modeling, the fact remains that rigorous scattering cannot be fully included in most models and coupling scattering models to quantum models continues to remain extremely challenging.

Efforts to include quantum effects in essentially particle-based models usually involve correction terms. Common methods of incorporating quantum effects are the density gradient formalism and the effective potential method [24]. The density gradient formalism is derived from the equation of motion for the one-particle Wigner function where quantum corrections are introduced by expressing the mean potential energy as a power series in Planck's constant h. The transport equation for the Wigner distribution function can now be written in the form of a modified BTE. In the effective potential method, a spatially localized wave packet is used as a representation of the electron where the size of the wave packet is defined roughly by the thermal deBroglie wavelength. The nonlocal form of the charge distribution introduces an effective potential when the inhomogeneous potential is introduced in the Hamiltonian. The generation of the effective potential determines the onset of quantization in the system due to the nonlocal nature of the potential. The quantum correction methods have been found to give an excellent match with the Poisson-Schrödinger solver for the case of carrier confinement and tunneling. More recently, attempts have been made to combine quantum corrections with the Monte Carlo technique [25], which is a numerical solution to the BTE. The results have been found to match well with the Schrödinger solution in the case of carrier confinement while a reasonably close match was observed for the case of tunneling. However, extension of this model to two and three dimensions remains, computationally tedious and difficult. Furthermore, the corrections are often heuristic and not based solely on first principles.

Quantum transport models often involve the solution to the Schrödinger equation and can be used to study current flow where the transport either is ballistic or includes limited scattering. Common models used to predict near-ballistic transport are quantum transmitting boundary model (QTBM) [26] and the quantum device analysis by mode evaluation (QDAME) [27]. QTBM involves formulating the boundary conditions for a given problem by calculating the transmission and reflection coefficients for a known boundary potential. These boundary conditions are then used in a discretized solution to obtain the wave function over the entire problem domain. Although this method is suitable for solving the Schrödinger equation for various boundary potentials, inclusion of dissipation due to scattering becomes very difficult. QDAME involves discretely sampling a device's density of states using standing wave boundary conditions. The standing waves are decomposed into traveling waves and injected from the contacts from which their occupancies are assigned.

Some of the contributing factors for problems associated with coupling quantum effects and scattering effects in device simulation are (i) time involved in converting new electronic device models including quantum effects into functioning simulation software and (ii) the immense computational resource requirement for accurate simulations of commercially important electronic devices. With device dimensions continuing to shrink, there is an increasing need for a simple model that can effectively couple quantum and scattering effects. The nonequilibrium Green's function formalism provides a framework for natural coupling of quantum and scattering effects. The source and drain contacts are coupled to the device through self-energy terms. The introduction of the Green's function for these terms eliminates the huge matrices that would normally be required to model the wave functions in an infinite reservoir. Instead matrices that are the size of the device Hamiltonian only are needed. In addition, the NEGF formalism allows for the rigorous incorporation of both elastic and inelastic scattering effects using the concept of Buttiker probes where scattering is treated as another contact, allowing it to be coupled to the device using the self-energy terms [28,29]. Unlike many other Schrödinger-based solver, the Green's function allows us to eliminate periodic boundary conditions leading to solutions for a device under bias. We present a brief synopsis of the formalism in Sec. 2 while a more thorough and detailed development can be found in [30] and [31].

Using the Green's function approach the performance of a silicon film and a Si/Ge heterostructure as thermoelectric materials are numerically investigated. Both structures are infinite in two directions and confined in the direction of transport. Therefore, the computational domain is one-dimensional. We are interested in calculating the electron transport due to a bias as a function of the confinement and scattering. Specifically, the IV characteristics can lead to direct calculation of the Seebeck coefficient and electrical conductance, which are desired for thermoelectric performance. By holding the two sides of the device at different temperatures a thermally induced electrical current is generated. A voltage is applied to bring the current to zero. This condition yields the Seebeck coefficient for the device. The electrical conductance is found from IV characteristics as the inverse of the slope of the linear region. We consider these performance characteristics in the presence of incoherent electron-phonon scattering, where the electrons interact inelastically with the surroundings. The energy lost or gained during this interaction with the lattice manifests itself in the form of phonons. The change in channel potential due to single electron charging effects is solved self consistently with the scattering model.

Effects believed to be important, but not addressed here, include energy-dependent scattering, inelastic electron-phonon scattering, crystal orientation, and full lattice structures. Although these effects are expected to affect the magnitude of transport, the trends of the predictions are not expected to change significantly. Furthermore, the application of NEGF to thermoelectric device is new and immature. Therefore, these simple models were chosen

to study the gross effects of reduced scale on thermoelectric material properties. The present study, therefore, will identify the important physical mechanisms responsible for determining the electrical properties of thermoelectric materials. We would also like to point out that coupled thermal-electrical solutions are rare, particularly those with quantum and scattering effects. Therefore, this approach represents an emerging technology to study multiphysics device performance. Some results involving the IV characteristics and the formalism used in the present study have previously been used in a conference proceedings [32]. Some results are repeated here where indicated for archival purposes and because of their importance in the prediction of the power factor $S^2\sigma$, which is the focus of the present work.

2 NEGF Formalism

2.1 Ballistic Development. In general, an isolated device and its energy levels are described using a Hamiltonian matrix H, where U is the Hartree potential and α is the energy eigenstate of the electron,

$$(H+U)\psi_\alpha(\vec{r}) = \varepsilon_\alpha\psi_\alpha(\vec{r}) \tag{1}$$

The electron density matrix in real space is given by [31]

$$\rho(\vec{r},\vec{r}') = \int_{-\infty}^{\infty} f_0(E-\mu)\,\delta(EI-H)dE \tag{2}$$

where f_0 is the Fermi function, and $\delta(EI-H)$ identifies the energies associated with the device Hamiltonian. Using an expansion of the δ function, we obtain

$$\delta(EI-H) = \frac{i}{2\pi}\{[(E-i0^+)I-H]^{-1} - [(E+i0^+)I-H]^{-1}\} \tag{3}$$

The two terms on the right-hand side can be reduced to

$$\delta(EI-H) = \frac{i}{2\pi}[G(E)-G^+(E)] \tag{4}$$

where the retarded Green's function is defined as

$$G(E) = [(E-i0^+)I-H]^{-1} \tag{5}$$

In general, the Green's function can be interpreted as the response of the Schrödinger equation to an impulse. In the present scenario, the impulse is essentially an electron density at a particular energy. In the energy domain, the Green's function gives the energy eigenvalues for the eigenstates that are occupied in response to the applied impulse. The density of states in real space is represented by the spectral function,

$$A(\vec{r},\vec{r}',E) = 2\pi i[G(E)-G^+(E)] \tag{6}$$

The diagonal elements of the spectral function represent the local electron density of states. Thus, the electron density matrix for an isolated device can also be written in the form

$$\rho(\vec{r},\vec{r}') = \frac{1}{2\pi}\int_{-\infty}^{\infty} f_0(E-\mu)A(E)dE \tag{7}$$

The density solution is solved self-consistently with Poisson's equation,

$$\nabla^2 U = -\frac{q}{\epsilon_s}(N_d - n) \tag{8}$$

where n is the real diagonal of the density matrix ρ and represents the real-space electron density along the device. N_d is the donor level, and ϵ_s is the permittivity.

Consider a simple nanotransistor consisting of source and drain contacts as in Fig. 1. Let μ_1 and μ_2 be the chemical potentials of the source and the drain where subsequent numerical subscripts will denote the source and drain, respectively. The energy distribution of electrons in the source and drain follows the Fermi-Dirac distribution where f_1 and f_2 are the corresponding Fermi functions. The difference in the chemical potentials of the source and drain, which results from the applied bias, causes electrons to flow between the contacts through the channel. When no scattering is included in the channel, the transport is ballistic in nature and the channel is expected to have zero resistance to current flow (infinite conductance). However, experimental measurements [33] have shown that the maximum measured conductance of a one-energy level channel approaches a limiting value $G_0 = 2q^2/\hbar = 51.6\ \mathrm{k\Omega}^{-1}$. The reason for this limit to conductance arises from the fact that current in a contact is carried by infinite transverse modes while the number of available modes in the channel is limited. Therefore, the density of states in the contact is spread over a large energy range while the channel density of states lies specifically between μ_1 and μ_2. Upon coupling the contact and the channel, some of the density of states from the contact spread into the channel while the channel loses some of its density of states to the contact. As a result, the coupling causes the density of states in the channel to spread out over a wider range of energy levels resulting in a reduction in the number of states lying between μ_1 and μ_2.This reduction limits the amount of current in the device.

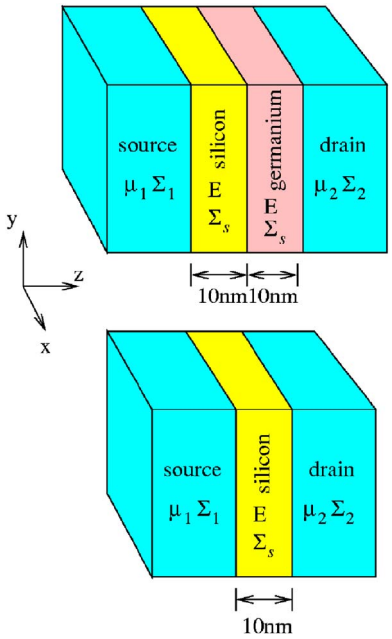

Fig. 1 Schematic representation of the nanodevice modeled in the simulation. *E* is the electron energy in the device while Σ_s is the scattering self-energy.

In the NEGF formalism, the coupling of the device to the source and drain contacts is described using self-energy matrices Σ_1 and Σ_2. The self-energy term can be viewed as a modification to the channel Hamiltonian to incorporate the boundary conditions. Accordingly, Eqs. (1) and (5) can be rewritten as

$$[H+U+\Sigma_1+\Sigma_2]\psi_\alpha(\vec{r}) = \varepsilon_\alpha\psi_\alpha(\vec{r}) \tag{9}$$

$$G(E) = [(E-i0^+)I-H-\Sigma_1-\Sigma_2]^{-1} \tag{10}$$

The self-energy term originates from the solution of the contact Hamiltonian. In this semi-infinite system, which is connected to the channel, there will be an incident wave from the channel as well as a reflected wave from the contact. The wave function at the interface is matched to conserve energy giving the boundary condition

$$\Sigma_i = -t\exp(ika) \tag{11}$$

where t is a result of the discretization and will be discussed later.

The broadening of the energy levels introduced by connecting the device to the source and drain contacts is incorporated through the functions Γ_1 and Γ_2 given by

$$\Gamma_1 = i(\Sigma_1 - \Sigma_1^+) \tag{12}$$

and

$$\Gamma_2 = i(\Sigma_2 - \Sigma_2^+) \tag{13}$$

The self-energy terms affect the Hamiltonian in two ways. The real part of the self-energy term shifts the device eigenstates or energy level while the imaginary part of Σ causes the density of states to broaden while giving the eigenstates a finite lifetime. The spectral function is defined as before in Eq. (6).

The electron density for the open system is now given as

$$\rho = \frac{1}{2\pi}\int_{-\infty}^{\infty} G^n(E)dE \tag{14}$$

where $G^n(E) \equiv G[\Gamma_1 f_1 + \Gamma_2 f_2]G^+$ for convenience and represents the electron density per unit energy. For plane wave basis functions, the current through the channel is calculated as the difference between the inflow and the outflow at any given contact

$$I_i = \frac{-q}{\hbar}\int_{-\infty}^{\infty} \mathrm{Tr}[\Gamma_i A]f_i - \mathrm{Tr}[\Gamma_i G^n]dE \tag{15}$$

where the i subscript indexes the contacts. For a two terminal device $I_1 = -I_2$.

2.2 Electron-Phonon Coupling. An electron in a device can interact with its surroundings elastically or inelastically, depending on the nature of surroundings. Elastic interactions occur when the surroundings are rigid leading to energy and momentum conservation. Such interactions are coherent in nature. Inelastic interactions occur when energy is dissipated through the emission or absorption of phonons, photons, etc. Such types of interactions are known as incoherent or phase-breaking processes. Inelastic scattering is, in general, difficult to model exactly. In this paper, we treat the phase-breaking scattering to be nearly elastic, i.e., $E \approx E + \hbar\omega \approx E - \hbar\omega$. The effect of scattering is incorporated into the coherent model discussed previously by treating it as another contact where electrons enter and leave the contact leading to no net current at that contact [31]. However, because the scattering terminal does not have a defined Fermi level, the scattering terms Σ_s and Γ_s have to be determined through other means. As such,

$$\Sigma_s^{\mathrm{in}}(\vec{r},\vec{r}',E) = D_0 G^n(\vec{r},\vec{r}',E) \tag{16}$$

$$\Gamma_s(E) = D_0 A(E), \quad \text{and} \quad \Sigma_s(E) = D_0 G(E) \tag{17}$$

D_0 is defined as the phonon correlation function and is calculated using the phonon deformation potential and the phonon wave vector β [31]

$$D_0(\vec{r},\vec{r}',\hbar\omega) = \sum_p \delta[E - \hbar\omega(\beta)]U_\beta(\vec{r})U_\beta^*(\vec{r}') \tag{18}$$

$$U_\beta(\vec{r}) = D_{\mathrm{adp}}\beta\sqrt{\frac{2\hbar}{\rho\omega\Omega}}\exp(i\beta\vec{r}) \tag{19}$$

D_{adp} is the acoustic deformation potential, ρ is the mass density, and Ω is the normalization volume. The values of D_0 represent the energy of the phonon with which the electrons scatter. Depending on the system temperature, there is a wide range of phonons with which electrons scatter. However in our model, we use a simplified case of the electrons interacting with phonons of a single frequency in an attempt to illustrate the effect of scattering on electron transport in devices. For example, $D_0 = 0.1\ \mathrm{eV}^2$ corresponds to a phonon energy of 20 meV [31]. This phonon energy is not related to the temperature of the device. In fact, the NEGF model does not include temperature within the system as temperature can be expressed only for a system that is in equilibrium. The only place where temperature is included in the model is in the source and drain Fermi functions. Instead, the phonon energy represents the dominant phonon frequency available for scattering [34]. In the present model, we assume D_{adp} is independent of the electron energy in the channel and corresponds to optical phonon scattering only, which is expected to be the dominant electron scatterer [35].

2.3 Numerical Scheme. The foregoing model is discretized on a uniform one-dimensional grid with a lattice spacing of a. Transport occurs parallel to the grid, which is also the confined direction. The Hamiltonian in Eq. (10) is an effective mass Hamiltonian, which averages the effects of the underlying periodic potential, and is given as the Laplacian operator. The discretized linear version is an $N \times N$ tridiagonal matrix given as

$$t\nabla^2 = [H] = \begin{bmatrix} Ec + 2t & -t & & \\ -t & Ec + 2t & -t & \\ & -t & Ec + 2t & \end{bmatrix} \tag{20}$$

where t is the coupling energy between adjacent nodes and is given in terms of the discretized spacing a and the effective mass m^* as

$$t = \frac{\hbar^2}{2m^* a^2} \tag{21}$$

The grid spacing a and grid size N is chosen such that the channel thickness $L = a(N-1)$. The grid spacing a must be chosen such that the coupling energy t is larger than the energy range of integration above the conduction band edge. In order to ensure current conservation, the energy eigenvalues of the Hamiltonian must be real. In order to meet this criterion, the Hamiltonian must be Hermitian. In the case where we are modeling a heterojunction, such as Si/Ge, there will be a spatially varying effective mass as well as conduction band edges. The spatial variation of the conduction band edges in the Hamiltonian allows for the automatic inclusion of boundary effects across interfaces. We employ the standard nonlinear control-volume approach [36] and require that the material interface lies at a node to ensure that the Hamiltonian remains Hermitian.

$$\nabla(t\nabla) = [H] = \begin{bmatrix} Ec_A + 2t_A & -t_A & & \\ -t_A & Ec_J + t_A + t_B & -t_B & \\ & -t_B & Ec_B + 2t_B & \end{bmatrix} \tag{22}$$

To initiate the solution, only the self-energy matrices for the source and drain contacts, which we can calculate directly, are used to obtain the values of $G(E)$. The self-energy term for the scattering contact is then calculated self-consistently from Eqs. (16) and (17) using the recently calculated values of $G(E)$. The source, drain and scattering self-energy terms are then used to obtain the final Green's function from which the net channel current is calculated as a difference in the inflow and outflow currents using Eq. (15) [29]. For the doping levels considered in this paper, the contacts are generally ohmic in nature, thus eliminating the need to model any barrier effects at the source and drain electrodes. The entire calculation is carried out self-consistently with Poisson's equation to account for the dependence of the channel potential on the electron density. This process is depicted in Fig. 2.

The computational requirements to solve for the current at a particular voltage depends on a number of factors. The grid size used in the present model consisted of 101 nodes. The resulting size of the Hamiltonian was a 101×101 matrix. For an energy range of 0–0.5 eV, we used 300 uniform integration steps. In the case of degenerate doping, however, the maximum contribution to current comes from energy values concentrated near the conduc-

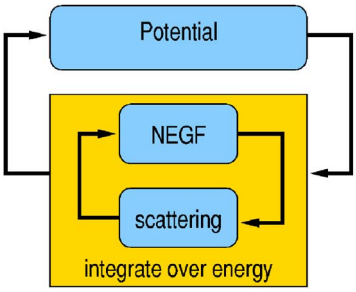

Fig. 2 Self-consistent iterations between the Green's function, scattering, and the potential. The inner process is integrated over energy.

tion band edge. In this case, care must be taken to choose an energy range close to the conduction band edge to ensure that the contribution from those energy steps is properly included. The matrix inversion in Eq. (10) was performed for each integration step, and the integration was performed self-consistently with the potential. This process was repeated for each voltage in the calculated IV characteristics.

To ensure numerical accuracy, first the number of integration steps was selected to ensure a suitable error. Next convergence of the potential calculation was set to an acceptable error. A relaxation of 0.2–0.5 on the density usually allowed convergence in about 20 iterations. The self-consistent approach can be used as long as the value of $U_o = q^2/\epsilon_0\epsilon_r$ as well as the value of the broadening Γ is comparable to k_BT. If U_o exceeds k_BT, the channel goes into the Coulomb blockade regime where the self-consistent method cannot be used anymore to solve for potential. The coupling energy t also has a similar effect as broadening and ensuring that $t \geq U_o$ will keep the channel in the self-consistent field regime. A large t implies that the grid spacing a is small, leading to more delocalization of the electron wave function, which, in turn, improves the accuracy of the self-consistent field calculation.

2.4 Physical Model. The silicon thin films modeled in our simulations were 10 nm thick as shown in Fig. 1. In the case of the Si/Ge heterostructure, each of the individual thin films were modeled as 10 nm thick layers each, leading to a combined thickness of 20 nm for the heterostructure. The bias applied on the devices ranged from 0–0.1 V on the drain.

3 Results and Discussion

3.1 Effects of Phase-Breaking Near Elastic Scattering. The channel current-voltage characteristics with incoherent, near-elastic scattering are shown in Fig. 3 for various scattering energies. Initially at zero bias, the source and drain Fermi levels are separated by a voltage V. The application of bias causes the energy levels of the drain to shift until the source and drain Fermi levels are equal. The channel current increases linearly during this time. Once the two Fermi levels align there are no additional energy states for the electron coming from the channel to occupy in the drain, causing the current to saturate. As mentioned in the Introduction, we have considered electron energy-independent near-elastic phonon scattering in this analysis. For this study, the free parameter D_0 was varied from a very low phonon energy of 0.2 meV to 60 meV, which is the optical phonon energy limit in the case of silicon, and the IV characteristics were collected. While $D_0 = 0.001$ eV^2 corresponding to phonon energy of 0.2 meV causes a reduction of 26% in the channel current, the current for $D_0 = 0.01$ eV^2 is found to decrease by 60% of the ballistic value. When D_0 is increased to 0.05 eV^2 corresponding to a phonon energy of 10 meV the current decreases further by 80%, demonstrating the importance of scattering effects on electron transport in small-scale devices. Further increase in phonon energy to 20 meV and 40 meV results in an additional decrease of only 5–10% in the current, indicating saturation in the amount of electron interaction with higher energy phonons. There is no additional decrease in the current for the 60 meV case.

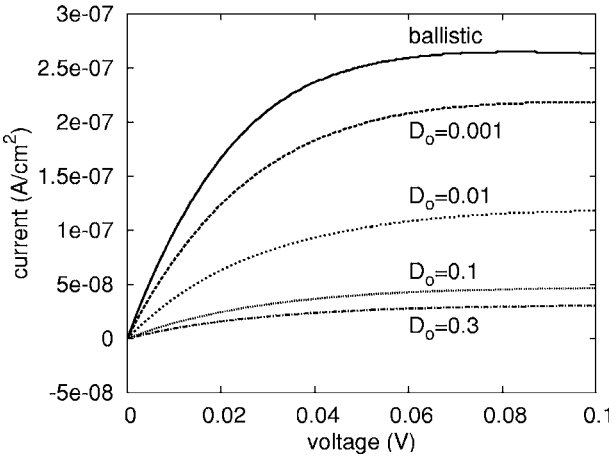

Fig. 3 Current versus voltage characteristics for incoherent, near-elastic scattering in a silicon thin film for $n = 5 \times 10^{18}$ cm^{-3}

3.2 Thermoelectric Effects in Silicon Thin Films. The Seebeck coefficient for silicon thin films were studied for various temperature ranges of the source and drain contacts while varying the doping in silicon. The source temperature was maintained constant at 300 K, whereas the drain contact was maintained a higher temperature relative to the source. The film thickness was 10 nm, and the applied bias ranged from 0 to 0.1 V. Figure 4 shows the current-voltage characteristics for a silicon thin film doped to electron concentration of 5×10^{18} cm^{-3} without scattering (ballistic case). The source-drain temperature difference ranged from 0 K to a maximum of 30 K. For low-bias conditions, the number of high-energy electrons generated in the drain contact is higher than the number of electrons arriving at the drain through the channel leading to negative current values. As the bias is increased gradually, more electrons from the source are drawn toward the drain due to the applied bias leading to higher inflow at the drain and positive current values. To estimate the Seebeck coefficient S, the applied bias is adjusted to obtain zero current.

For the case of near-elastic scattering, the value of the Seebeck coefficient was found to be independent of the scattering strength

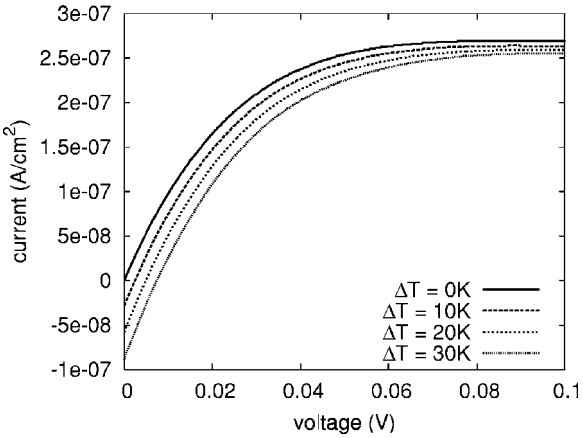

Fig. 4 Temperature-dependent current-voltage characteristics of a silicon thin film for a channel temperature difference of 0–30 K without scattering: $n = 5 \times 10^{18}$ cm^{-3}

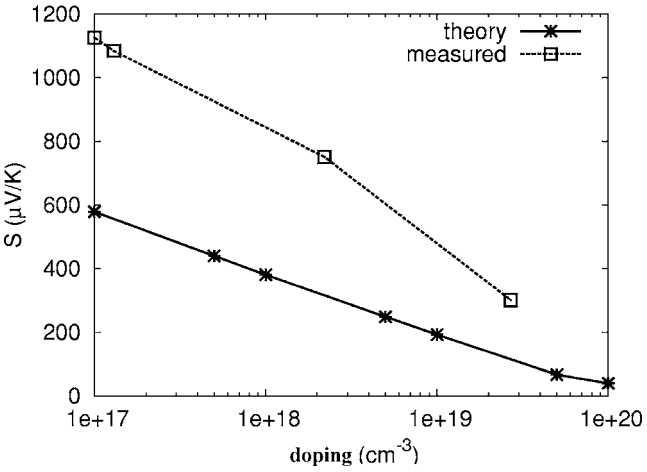

Fig. 5 Predicted versus measured [39] values of Seebeck coefficient for silicon at 300 K as a function of doping levels

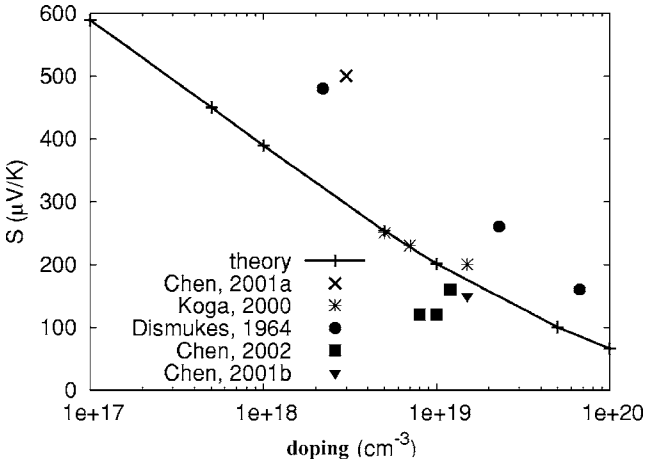

Fig. 6 Predicted versus measured Seebeck [5,6,41–43] coefficient for ballistic Si(10 nm)/Ge(10 nm) superlattice with doping

D_0. However, S is a function of doping. The conduction band edge and Fermi level are related to the doping level in the semiconductors by the carrier density

$$n = N_c \exp\left(-\frac{E_c - E_f}{k_B T}\right) \tag{23}$$

Here, N_c is the effective density of states at the conduction band edge and E_c and E_f the conduction band edge and Fermi level, respectively [37]. Varying the relative values of the conduction band edge and the Fermi level allows us to vary the doping level in the semiconductors. For all doping levels, the Seebeck coefficient was found to change almost linearly as a function of the temperature difference for small temperature changes. However, this does not hold true as the temperature difference across the device is increased. Yang et al. [38] studied the anisotropic thermoelectric properties of superlattices. They reported that although the Seebeck coefficient does not exhibit very high anisotropy between the in-plane and cross-plane directions, the cross-plane Seebeck coefficient rises rapidly with device temperature. The value of Seebeck coefficient in our calculations changes by $\sim 4-5\ \mu$V/K for a temperature range of 0–30 K. This small change in S allows us to report an average value rather than the slope of the Seebeck voltage versus ΔT plot (Fig. 4).

Figure 5 shows the averaged predicted and measured Seebeck coefficient values for silicon for various doping levels in all temperature ranges considered. The predicted values of S differ from the experimentally measured values [39] approximately by a factor of 2. Although there is limited experimental data for the Seebeck coefficient for silicon thin films, it must be noted that the trends predicted by our model match the trends of the experimental data for bulk silicon.

3.3 Thermoelectric Effects in Si/Ge Thin Films. The thermoelectric properties of Si/Ge heterostructures were studied in a manner similar to silicon by maintaining the drain at higher temperatures than the source. Quantum confinement effects can be found in [40] and in a forthcoming paper derived from [40]. Each of the semiconductor thin films was modeled as 10 nm thick, leading to a combined thickness of 20 nm for the heterojunction. Similar to silicon, the doping in silicon and germanium was varied by changing the relative values of E_c and μ. The amount of doping was modeled to be constant throughout the two materials. The predicted values of the Seebeck coefficients with doping is shown in Fig. 6. Although there is a large spread in the experimentally measured results for various doping levels in the superlattices, the results from our model show fair agreement with the measured values. We do not expect our results to match the experimental data exactly for a number of reasons: (i) although our model incorporates quantum effects in the form of discrete energy states in the channel, it does not include the additional effect of electron confinement induced by the quantum well Si-Ge-Si superlattice. (ii) The superlattices used in the experiments consist of 300–1200 alternating layers of silicon and germanium films whose thicknesses are of the order of a few angstroms while our model consists of a single heterojunction where each film is 10 nm thick. (iii) The values used for the effective mass for silicon and germanium correspond to bulk values while the experiments were performed on single crystalline epitaxial layers. It was seen in our simulations that the value of the effective mass used in the calculations significantly affects the current-voltage characteristics. For film thicknesses of the order of few nanometers as used in our calculations, both silicon and germanium can be considered to be single crystals, allowing us to use the effective mass for that particular orientation. (iv) We have used the Fermi-Dirac function to model the inflow of electrons supplied by the source and drain contacts. This means that the contacts will supply electrons having a continuum energy distribution in all directions while entering the channel. However, for film thicknesses used in our simulations, additional electron confinement due to the reduced dimensionality of the 2D film is expected causing the electrons entering the channel to have discrete energy levels in the direction of transport. This effect of reduced dimensionality can be modeled by using a 2D Fermi function that will treat the electrons entering from the contacts as having infinite boundary conditions in the bulk directions and discrete energy states in the direction of confinement. It is expected that incorporating this effect of reduced dimensionality in our model will increase the local density of states per unit volume at the Fermi level leading to an increase in the predicted Seebeck coefficient.

Conductivity values for each value of D_0 were calculated from the slope of the linear portion of the IV characteristics.

$$\sigma = \frac{dI}{dV} L \tag{24}$$

where L is the channel thickness. It was seen that inclusion of electron-phonon scattering caused a significant drop in the current conducted through the channel indicating increased resistance to current flow with scattering. The $S^2\sigma$ value was calculated using the conductivity values predicted for each level of scattering along with the Seebeck coefficient obtained for each doping level considered. The decrease in conductivity led to an overall decrease in the power factor as demonstrated from the reduction in $S^2\sigma$ values with increasing scattering seen in Fig. 7. However, the $S^2\sigma$ values

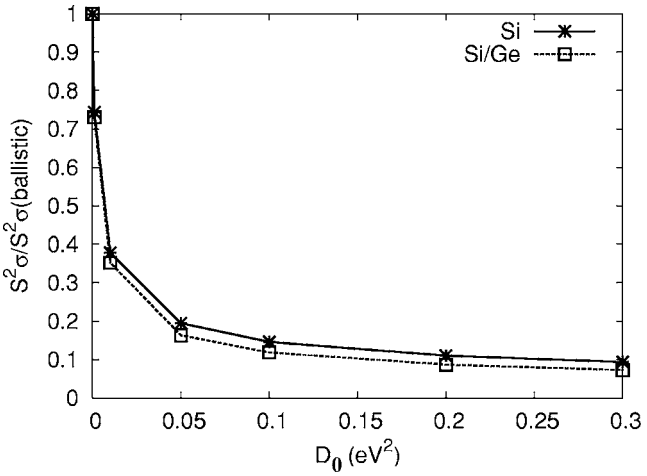

Fig. 7 Change in $S^2\sigma$ with incoherent electron-phonon scattering for silicon thin films and Si/Ge heterojunctions: $N_{d,\mathrm{Si}}=5\times10^{18}$ cm^{-3}, $N_{d,\mathrm{SiGe}}=5\times10^{18}$ cm^{-3}

of Si/Ge were found to be two times greater than the silicon thin films for the same doping level.

4 Conclusions

The nonequilibrium Green's function formalism was used to couple quantum effects and scattering effects in a 10 nm thick silicon film. The model was used to demonstrate near-elastic, phase-breaking electron-phonon scattering effects in very small-scale devices. A 26–90% decrease in current was noted when phonon scattering was included. The NEGF formalism was used to study thermoelectric behavior of electrons in silicon thin films and Si/Ge heterojunction. The predicted Seebeck coefficient values for silicon and Si/Ge heterojunctions matched well with the experimentally measured values. Inclusion of electron-phonon scattering in the model increased the electrical resistance causing the value of $S^2\sigma$ for silicon thin film and the heterojunction to decrease by 26–90% of their ballistic values. However, the $S^2\sigma$ values for the Si/Ge heterojunction was found to be enhanced compared to the $S^2\sigma$ values for silicon thin films. Current research efforts are focused toward incorporating electron energy-dependent inelastic electron-phonon scattering as well as phonon transport through devices to study all coupled effects present in the prediction of ZT for devices and materials.

Acknowledgment

We are grateful to Prof. Supriyo Datta, Department of Electrical and Computer Engineering, Purdue University, for providing us with a preprint of his book [31] on which much of this work is based. This research was funded through a Vanderbilt Discovery Grant and a Vanderbilt Institute of Nanoscale Science and Engineering (VINSE) fellowship.

References

[1] Hicks, L. D., and Dresselhaus, M. S., 1993, "Effect of Quantum-Well Structures on the Thermoelectric Figure of Merit," Phys. Rev. B, **47**(19), pp. 12727–12731.
[2] Hicks, L. D., Harman, T. C., and Dresselhaus, M. S., 1993, "Use of Quantum-Well Superlattices to Obtain a High Figure of Merit From Nonconventional Thermoelectric Materials," Appl. Phys. Lett., **63**(23), pp. 3230–3232.
[3] Tritt, T. M., 2001, *Recent Trends in Thermoelectric Materials Research III: Semiconductors and Semimetals*, Academic Press, New York, Vol. 3.
[4] Simkin, M. V., and Mahan, G. D., 2000, "Minimum Thermal Conductivity of Superlattices," Phys. Rev. Lett., **84**(5), pp. 927–930.
[5] Koga, T., Cronin, S. B., Dresselhaus, M. S., Liu, J. L., and Wang, K. L., 2000, "Experimental Proof-of-Principle Investigation of Enhanced $Z_{3D}T$ in 001 Oriented Si/Ge Superlattices," Appl. Phys. Lett., **77**(10), pp. 1490–1492.
[6] Yang, B., Liu, J., Wang, K., and Chen, G., 2001, "Characterization of Cross-Plane Thermo-Electric Properties of Si/Ge Superlattices," *Proc. of 20th International Conference on Thermoelectrics (ICT)*, Beijing, China, June, pp. 344–347.
[7] Yang, B., Liu, J. L., Wang, K. L., and Chen, G., 2002, "Simultaneous Measurements of Seebeck Coefficient and Thermal Conductivity Across Superlattice," Appl. Phys. Lett., **80**(10), pp. 1758–1760.
[8] Harman, T. C., Taylor, P. J., Walsh, M. P., and La Forge, B. E., 2002, "Quantum Dot Superlattice Thermoelectric Materials and Devices," Science, **297**(27), pp. 2229–2232.
[9] Venkatasubramanian, R., Siivola, E., Colpitts, T., and O'Quinn, B., 2001, "Thin-Film Thermoelectric Devices With High Room-Temperature Figures of Merit," Nature (London), **413**(11), pp. 597–602.
[10] Chen, G., 1998, "Thermal Conductivity and Ballistic-Phonon Transport in the Cross-Plane Direction of Superlattices," Phys. Rev. B, **57**(23), pp. 14958–14973.
[11] Chen, G., 1999, "Phonon Wave Heat Conduction in Thin Films and Superlattices," ASME J. Heat Transfer, **121**, pp. 945–953.
[12] Dresselhaus, M. S., 2003, "Nanostructures and Energy Conversion Devices," *Proc. of 2003 Rohsenow Symposium on Future Trends of Heat Transfer*, Cambridge, MA, May, pp. 1–3.
[13] Rahman, A., Ghosh, A., and Lundstrom, M., "Assessment of Ge n-MOSFETs by Quantum Simulation," IEEE International Electron Devices Meeting (IEDM) Technical Digest, pp. 19.4.1–19.4.4, December 2003.
[14] Mazumder, P., Kulkarni, S., Bhattacharya, M., Sun, J. P., and Haddad, G. I., 1998, "Digital Circuit Applications of Resonant Tunneling Devices," Proc. IEEE, **86**(4), pp. 664–686.
[15] Cahill, D. G., Ford, W. K., Goodson, K. E., Mahan, G. D., Majumdar, A., Maris, H. J., Merlin, R., and Phillpot, S. R., 2003, "Nanoscale Thermal Transport," J. Appl. Phys., **93**(2), pp. 793–818.
[16] Asheghi, M., Leung, Y. K., Wong, S. S., and Goodson, K. E., 1997, "Phonon-Boundary Scattering in Thin Silicon Layers," Appl. Phys. Lett., **71**(13), pp. 1798–1800.
[17] Zhou, J. H., Jin, C. G., Li, X. G., and Shi, L., 2005, "Thermoelectric Properties of Individual Electrodeposited Bismuth Telluride Nanowires," Appl. Phys. Lett., **87**(13), p. 133109.
[18] Blotekjaer, K., 1970, "Transport Equations for Electrons in Two-Valley Semiconductors," IEEE Trans. Electron Devices, **17**(1), pp. 38–47.
[19] Lugli, P., 1990, "The Monte Carlo Method for Semiconductor Device and Process Modeling," IEEE Trans. Comput.-Aided Des., **9**(11), pp. 1164–1176.
[20] Mazumder, S., and Majumdar, A., 2001, "Monte Carlo Study of Phonon Transport in Solid Thin Films Including Dispersion and Polarization," ASME J. Heat Transfer, **123**(4), pp. 749–759.
[21] Lai, J., and Majumdar, A., 1996, "Concurrent Thermal and Electrical Modeling of Sub-Micrometer Silicon Devices," J. Appl. Phys., **79**(9), pp. 7353–7361.
[22] Raman, A., Walker, D. G., and Fisher, T. S., 2003, "Simulation of Nonequilibrium Thermal Effects in Power LDMOS Transistors," Solid-State Electron., **47**(8), pp. 1265–1273.
[23] Murthy, J. Y., and Mathur, S. R., 2002, "Computation of Sub-Micron Thermal Transport Using an Unstructured Finite Volume Method," ASME J. Heat Transfer, **124**(6), pp. 1176–1181.
[24] Asenov, A., Watling, J. R., Brown, A. R., and Ferry, D. K., 2002, "The Use of Quantum Potentials for Confinement and Tunnelling in Semiconductor Devices," J. Comput. Electron., **1**(4), pp. 503–513.
[25] Tang, T., and Wu, B., 2004, "Quantum Correction for the Monte Carlo Simulation Via the Effective Conduction-Band Edge Equation," Semicond. Sci. Technol., **19**(1), pp. 54–60.
[26] Lent, C. S., and Kirkner, D. J., 1990, "The Quantum Transmitting Boundary Method," J. Appl. Phys., **67**(10), pp. 6353–6359.
[27] Laux, S. E., Kumar, A., and Fischetti, M. V., 2002, "Ballistic Fet Modeling Using QDAME: Quantum Device Analysis by Modal Evaluation," IEEE Trans. Nanotechnol., **1**(4), pp. 255–259.
[28] Datta, S., 1989, "Steady-State Quantum Kinetic Equation," Phys. Rev. B, **40**(8), pp. 5830–5833.
[29] Datta, S., 1990, "A Simple Kinetic Equation for Steady-State Quantum Transport," J. Phys.: Condens. Matter, **2**(40), pp. 8023–8052.
[30] Datta, S., 2000, "Nanoscale Device Modeling: The Green's Function Method," Superlattices Microstruct., **28**(4), pp. 253–278.
[31] Datta, S., 2005, *Quantum Transport: Atom to Transistor*, Cambridge University Press, Cambridge, MA.
[32] Bulusu, A., and Walker, D. G., 2005, "Modeling of Electron Transport in Thin Films With Quantum and Scattering Effects," ASME/Pacific Rim Technical Conference and Exhibition on Integration and Packaging of MEMS, NEMS and Electronic Systems, San Francisco, July, ASME Paper No. IPACK2005–73212.
[33] Szafer, A., and Stone, A. D., 1989, "Theory of Quantum Conduction Through a Constriction," Phys. Rev. Lett., **62**(3), pp. 300–303.
[34] Lundstrom, M., and Ren, Z., 2002, "Essential Physics of Carrier Transport in Nanoscale MOSFETs," IEEE Trans. Electron Devices, **49**(1), pp. 133–141.
[35] Tien, C.-L., Majumdar, A., and Gerner, F. M., eds. 1998, *Microscale Energy Transport*, Taylor & Francis, New York, pp. 3–94.
[36] Patankar, S. V., 1980, *Numerical Heat Transfer*, Taylor and Francis, New York.
[37] Muller, R., and Kamins, T., 1986, *Device Electronics for Integrated Circuits*, Wiley, New York.
[38] Yang, B., Liu, W. L., Liu, J. L., Wang, K. L., and Chen, G., 2002, "Measurements of Anisotropic Thermoelectric Properties in Superlattices," Appl. Phys.

Lett., **81**(19), pp. 3588–3590.
[39] Geballe, T. H., and Hull, G. W., 1955, "Seebeck Effect in Silicon," Phys. Rev., **98**(4), pp. 940–948.
[40] Bulusu, A., and Walker, D. G., 2006, "Effect of Quantum Confinement on Thermoelectric Properties of 2D and 1D Semiconductor Thin Films," *Proc. of ITherm*, San Diego, July.
[41] Dismukes, J. P., Ekstrom, L., Steigmeier, E. F., Kudman, I., and Beers, D. S., 1964, "Thermal and Electrical Properties of Heavily Doped Ge-Si Alloys up to 1300 k," J. Appl. Phys., **35**(10), pp. 2899–2907.
[42] Liu, W. L., Tasciuc, T. B., Liu, J. L., Taka, K., Wang, K. L., Dresselhaus, M. S., and Chen, G., 2001, "In-Plane Thermoelectric Properties of Si/Ge Superlattices," *Proc. of 20th International Conference on Thermoelectrics (ICT)*, Beijing, China, July, pp. 340–343.
[43] Liu, W. L., Chen, G., Liu, J. L., and Wang, K. L., 2002, "Quantum and Classical Size Effects on Thermoelectric Transport in Si/Ge Superlattices," *Proc. of 21st International Conference on Thermoelectrics (ICT)*, pp. 130–134.